Marine Nitrous Oxide Emissions from Three Eastern Boundary Upwelling Systems Inferred from Atmospheric Observations

Marine Nitrous Oxide Emissions from Three Eastern Boundary Upwelling Systems Inferred from Atmospheric Observations

A.L. Ganesan[1], M. Manizza[2], E.J. Morgan[2], C.M. Harth[2], E. Kozlova[3], T. Lueker[2], A.J. Manning[4], M.F. Lunt[5], J. Mühle[2], J.V. Lavric[6], M. Heimann[6,7], R.F. Weiss[2], M. Rigby[8]

[1]School of Geographical Sciences, University of Bristol, UK.

[2]Scripps Institution of Oceanography, University of California San Diego, USA.

[3]University of Exeter, College of Life and Environmental Sciences, UK.

[4]Hadley Centre, Met Office, UK.

[5]School of Geoscience, University of Edinburgh, UK.

[6]Max Planck Institute for Biogeochemistry, Germany.

[7]Institute for Atmospheric and Earth System Research (INAR) / Physics, University of Helsinki, Finland.

[8]School of Chemistry, University of Bristol, UK.

Corresponding author: Anita Ganesan (anita.ganesan@bristol.ac.uk)

Key Points:

- Eastern Boundary Upwelling System (EBUS) N_2O emissions are episodic and methods are needed to capture their variability in space and time
- Previous estimates based on sparse measurements can be inaccurate
- N_2O emissions from the northern California upwelling system vary with PDO phase

Abstract

Eastern Boundary Upwelling Systems (EBUSs) are coastal hotspots of the potent greenhouse gas nitrous oxide (N_2O). However, estimates of their emissions suffer from large uncertainties due to their significant spatial and temporal heterogeneity. Here, we derive the first multi-year, monthly resolution N_2O emissions from three of the four major EBUSs using high-frequency coastal atmospheric measurements and an inverse method. We find average combined N_2O emissions from the northern California, Benguela and southern Canary upwelling systems to be 57.7 (51.4-63.9) Gg-N yr^{-1}. We also find an offshore region near the Benguela EBUS that exhibits large pulses of emissions with emissions that reach 677 Gg-N yr^{-1} in one month. Our findings highlight that atmospheric measurements coupled with inverse modeling can capture the large variability in EBUS emissions by quantifying emissions over large spatial distances and over long time periods compared to previous methods using traditional oceanographic measurements.

Plain Language Summary

Eastern Boundary Upwelling Systems (EBUSs) are important emissions hotspots of marine nitrous oxide to the atmosphere, where it acts as a greenhouse gas and ozone depleting substance. Emissions from the EBUSs are highly episodic and most previous estimates are snapshots derived from ship-based measurements. The variability in emissions combined with the sparsity of measurements makes EBUS emission estimates highly uncertain. Here, we use multi-year, near-continuous atmospheric measurements from coastal stations and an inverse modeling framework to derive emissions from three of the four major EBUSs. Our results

quantify the significant spatial and temporal variability in emissions, which is not well-represented in global studies of marine nitrous oxide emissions.

1 Introduction

Nitrous oxide (N_2O) is a potent greenhouse gas and a major ozone depleting substance (Myhre et al., 2013; Ravishankara et al., 2009). Estimates of emissions from the ocean exhibit significant spread (Battaglia & Joos, 2018; Ciais et al., 2013) due to the challenge in simulating complex biogeochemical pathways, capturing large spatial and temporal variability and due to sparse measurements. High concentrations of N_2O in the ocean are found in regions known as Eastern Boundary Upwelling Systems (EBUSs), where high productivity rates due to upwelling lead to low oxygen conditions, favoring N_2O production. EBUSs are often associated with ocean oxygen minimum zones (OMZs) (Capone & Hutchins, 2013; Oschlies et al., 2018). Strong upwelling in these regions also provides an efficient pathway for release of N_2O into the atmosphere (Nevison et al., 2004). The four major EBUSs are associated with the California (eastern North Pacific), Benguela (eastern South Atlantic), Canary (eastern tropical North Atlantic), and Humboldt (eastern tropical South Pacific) Current Systems (Chavez & Messié, 2009).

Previous studies have shown that coastal areas can emit disproportionally large amounts of N_2O compared to their fraction of global area (e.g., Naqvi et al., (2010)). However, previous estimates are based on methods that are not able to capture the significant spatial and temporal heterogeneity in coastal upwelling and thus may be inaccurate. Coastal upwelling events are episodic, occurring on the timescale of hours to days (Nevison et al., 2004) and with spatial

extent that can vary seasonally and year-to-year. Previous methods to quantify EBUS N_2O emissions have used sparse ship-based measurements of seawater N_2O concentration (e.g., Arévalo-Martínez et al., 2015; Capelle & Tortell, 2016; Fenwick & Tortell, 2018; Frame et al., 2014; Kock et al., 2008; Wittke et al., 2010) or models employing climatological concentration fields and estimates of air-sea exchange (e.g., Buitenhuis et al., 2018; Nevison et al., 2004). Both methods suffer the challenge of capturing variability by being snapshots or by being based on composite N_2O concentration fields, which have combined sparse measurements over decades. These limitations have resulted in large uncertainties in estimates of EBUS emissions.

Here, we present the first timeseries of spatially resolved estimates of EBUS N_2O emissions derived from multi-year records of high-frequency atmospheric measurements and an inverse method, thus capturing variability in time and space. We used data from three coastal stations near the northern California, Benguela and southern Canary (Mauritanian) EBUSs (no suitable atmospheric measurements are available near the Peruvian EBUS). The dataset was comprised of 15 years of atmospheric dry air mole fraction measurements from Trinidad Head, California (THD, Prinn et al., 2018), two years from the Namib Desert Atmospheric Observatory (NDAO, Morgan et al., 2015) and four years from the Cape Verde Atmospheric Observatory (CVAO). Measurements were coupled with the atmospheric transport model NAME (Numerical Atmospheric Modelling Environment) (Jones et al., 2006) at 3-hourly and up to 12 km spatial resolution and a hierarchical Bayesian inverse method (Ganesan et al., 2014; Lunt et al., 2016). We used a global ocean model, ECCO2-Darwin (described in Manizza et al., (2019) and updated to include N_2O fluxes using Manizza et al., (2012); Nevison et al., (2003); Wanninkhof, (1992) as described in the SI) at approximately 18 km and monthly resolution to provide *a priori* ocean N_2O fluxes for the inversion.

The near-continuous nature of atmospheric measurements means that if wind directions are favorable, many episodic events can be captured in the measurement record and assessed over time. Previous studies (Lueker, 2004; Morgan et al., 2019; Nevison et al., 2004) that have used atmospheric measurements to estimate coastal emissions have had to attribute emissions to pre-defined source regions and relied on measurements sampling the ocean to not be conflated with terrestrial sources. We show that interpreting atmospheric measurements without a spatially and temporally resolved atmospheric transport model can lead to emissions magnitudes and their spatial distribution to be incorrectly derived.

2 Results

The first spatially resolved timeseries spanning multiple years of EBUS N_2O emissions from three of the four major EBUSs are presented. Mean emission maps for the northern California, Benguela and southern Canary EBUSs are shown in **Figs. 1 and S1**. Area-integrated emissions for each month for the coastal (0-150 km from coast) areas defined in **Fig. 1** are shown in **Fig. 2**. Estimates from previous studies are provided in **Table S1**. Due to the episodic and variable nature of EBUS emissions, only a few direct comparisons to previous studies are possible.

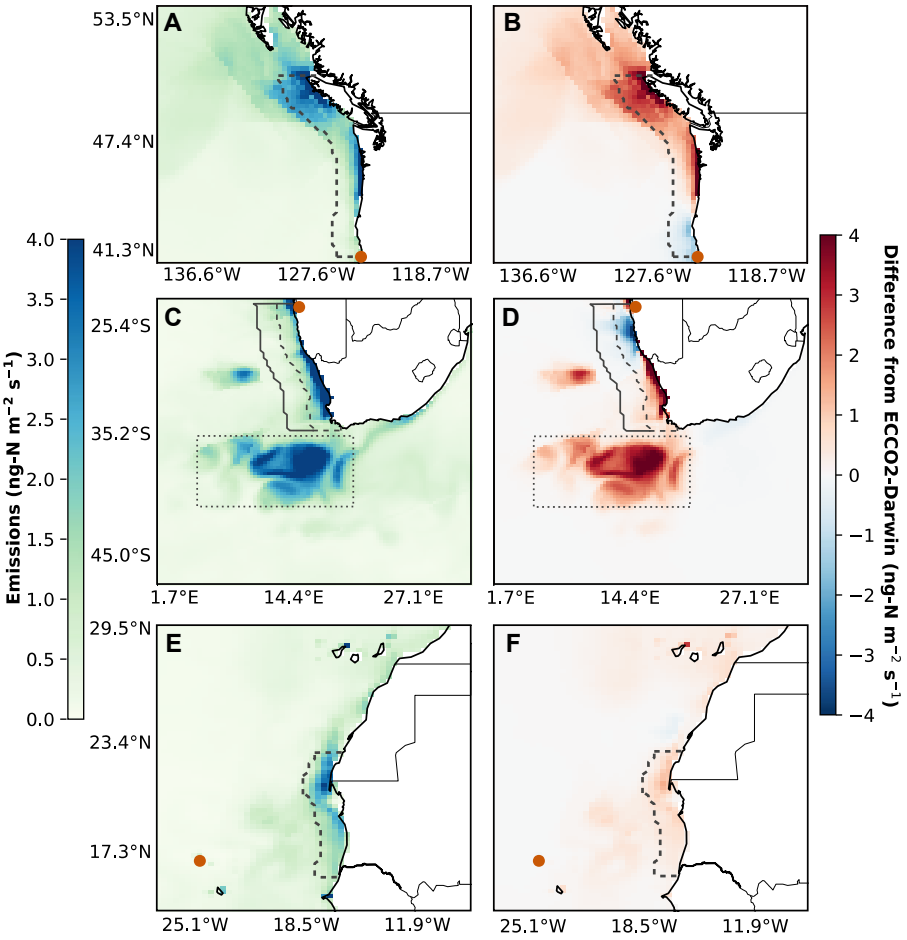

Fig. 1. Spatial distribution of N_2O emissions inferred from atmospheric measurements. **(a,c,e)** Mean emissions and **(b,d,f)** mean difference from the ocean model ECCO2-Darwin in ng-N m^{-2} s^{-1} for the **(a,b)** northern California, **(c,d)** Benguela, and **(e,f)** southern Canary EBUSs over the time periods of each study. Atmospheric measurement stations used in each of these regions are indicated by the orange circles. Dashed and solid grey boxes (in **c,d**) denote 0-150km and 150-400km distances from the coast, respectively. The dotted box in **(c,d)** represents an open ocean area near the Benguela EBUS. These boxed regions denote the areas over which emissions have been aggregated. Results were derived for both the land and ocean but are shown only for the ocean for clarity. Results for both land and ocean and the *a priori* emissions fields are shown in **Fig. S1**.

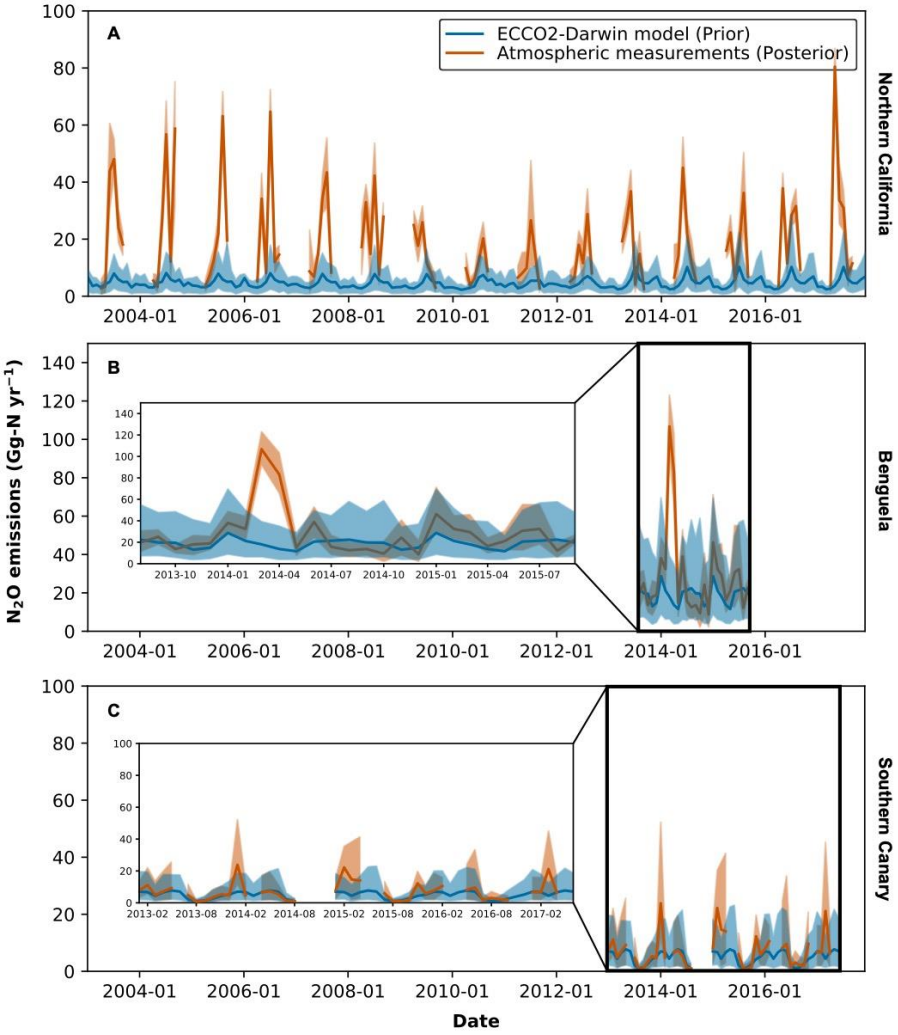

Fig. 2. Time series of coastal ocean N_2O emissions. Emissions in Gg-N yr^{-1} are shown for the **(a)** northern California **(b)** Benguela, and **(c)** southern Canary EBUSs. Emissions derived from atmospheric measurements are shown in orange with the 95% confidence interval in orange shading and are only shown for months that are well-constrained by atmospheric measurements. *A priori* emissions and uncertainty from the ocean model ECCO2-Darwin are shown in blue for all months. Gaps in the *a priori* timeseries indicate months where no measurements are available. The spatial areas over which emissions have been aggregated are shown by the 0-150 km boxes in **Fig. 1.** Insets in **(b,c)** zoom-in over the results.

2.1 Northern California (41°-50°N)

The northern California EBUS exhibits seasonality in wind patterns. The influence of oceanic emissions is observed in the atmospheric mole fraction record of N_2O at THD each year from April through September. Outside of these months, wind directions are generally not favorable for observing an ocean source with sufficient sensitivity. Furthermore, the northerly winds needed to induce upwelling are found during these months, with winter months exhibiting reduced upwelling or downwelling conditions (Huyer, 1983). We therefore present emissions only over the April through September inversion period.

Mean (95% confidence interval) area-integrated coastal ocean emissions from 2003-2017 are 19.2 (18.5-19.9) Gg-N yr^{-1} (**Fig. 2**). If it is assumed that emissions outside of April through September are negligible, a lower-bound of mean annual emissions is 9.6 (9.3-10.0) Gg-N yr^{-1}. We find that maximum monthly emissions reach 80.4 Gg-N yr^{-1}, a value that is almost five times larger than the mean, highlighting the large variability in emissions that could be missed with sporadic sampling.

The increase in emissions relative to the ECCO2-Darwin model occurs primarily off the coast of Oregon and Washington, USA and British Colombia, Canada (**Fig. 1**). Fluxes off the coast of Vancouver derived from ship-based measurements during the time period of this analysis (Capelle & Tortell, 2016; Fenwick & Tortell, 2018) show Vancouver to be a region of strong upwelling N_2O emissions with mean emissions similar to those derived here (**Table S1**). Our mean per-area emissions of 2.4 ng-N m^{-2} s^{-1} is however 80% larger than estimated in (Nevison et al., 2004) using composite ΔpN_2O fields for the same latitude band (**Table S1**),

indicating that using climatological fields to derive emissions could be inaccurate for capturing variable sources.

Two previous studies (Lueker, 2004; Nevison et al., 2004) used 2000-2002 atmospheric data from THD to derive N_2O emissions using an atmospheric box model. There are several limitations with these previous approaches. First, estimated emissions were highly sensitive to atmospheric model inputs, which included atmospheric dilution, wind speed, planetary boundary layer height (PBLH) and the spatial footprint assigned to the mole fraction enhancement. Atmospheric dilution is described in Nevison et al., (2004) to be the least quantified parameter and a range of values were assigned. Wind speed and PBLH inputs were averages over the spatial area and the two studies attributed emissions derived from the same data to different pre-defined spatial areas (i.e., 35°-50°N and 41°-50°N). Third, these estimates used depletion in atmospheric potential oxygen (APO), which is derived from measurements of the O_2/N_2 ratio and carbon dioxide, to determine times of upwelling (Lueker et al., 2003). Corresponding enhancements in N_2O mole fraction were then used to infer oceanic N_2O emissions. As shown in **Fig. S2**, N_2O mole fraction enhancements during upwelling events at THD could also overlap with enhancements from terrestrial (natural soil, Saikawa et al., 2013) and anthropogenic (Janssens-Maenhout et al., 2019) sources and therefore N_2O enhancements should not be solely attributed to marine emissions. The atmospheric transport model used in this study uses three-dimensional meteorological fields at high spatial and temporal resolution to quantify the footprint of atmospheric enhancements and the inverse method solves for both land and marine emissions to minimize misattribution of enhancements.

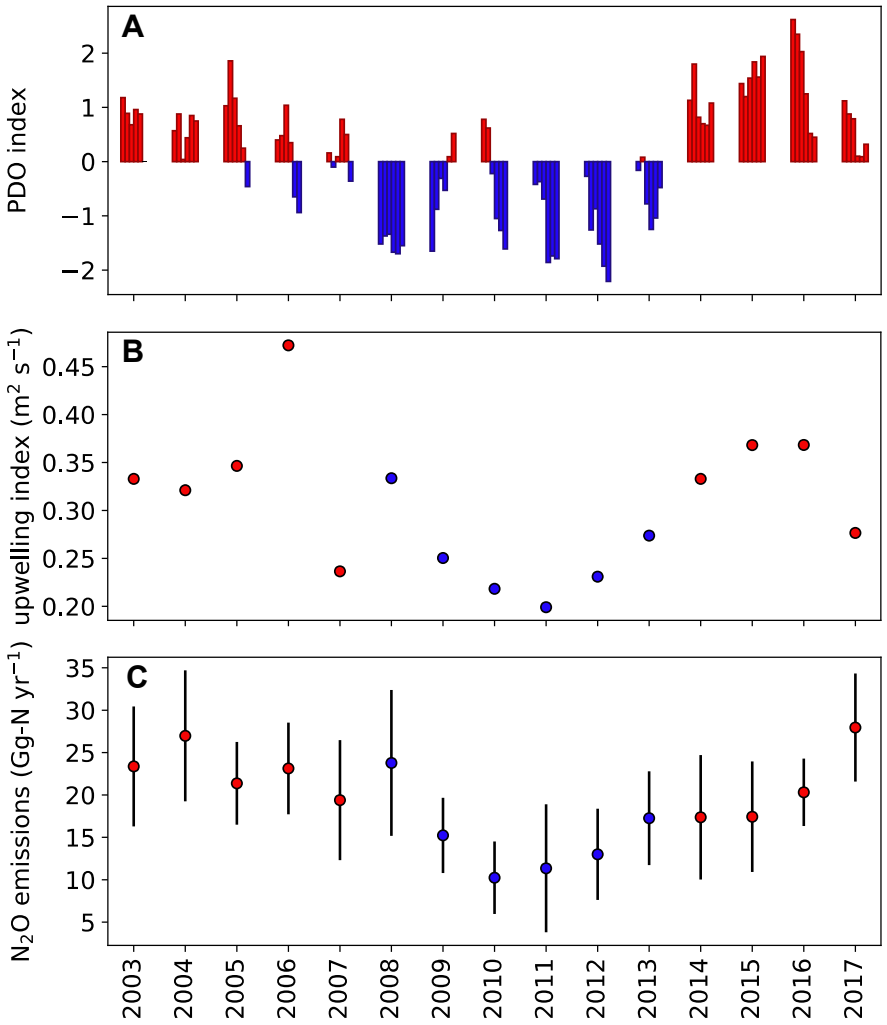

Fig. 3. Climate indices and N_2O emissions for the northern California EBUS for April-September. (a) Pacific Decadal Oscillation (PDO) index (Mantua et al., 1997), **(b)** Mean Coastal Upwelling Transport Index (m^2 s^{-1}) over 44°-47°N (NOAA Southwest Fisheries Science Center), **(c)** Mean N_2O emissions and uncertainty as in **Fig. 2a**. **(b,c)** are colored according to warm (red) and cool (blue) PDO phases.

Marine N_2O emissions are governed by physical and biogeochemical drivers, which can vary with climatic conditions (Capone & Hutchins, 2013). The Pacific Decadal Oscillation (PDO) is the leading mode of variability in sea surface temperatures (SSTs) in the North Pacific

(**Fig. 3a**). Variability in SSTs can drive changes in N_2O emissions through changes in solubility, controlling the amount of N_2O outgassing to the atmosphere, as well as through changes in upwelling and ventilation (Manizza et al., 2012). Warm and cool PDO phases correspond to higher and lower coastal SSTs, respectively and higher and lower coastal upwelling strength, respectively (**Fig. 3b**).

As we have derived estimates of N_2O emissions from the northern California EBUS spanning nearly two decades, we are for the first time able to correlate patterns in N_2O emissions with climatic drivers. We find that N_2O emissions broadly correlate with the phase of the PDO (**Fig. 3c**). Emissions during April through September of warm phase PDO years are 22.8 (21.4-24.2) Gg-N yr^{-1} from 2003-2007 and 20.1 (19.5-22.1) Gg-N yr^{-1} from 2014-2017, and during the cool phase of 2008-2013 are 15.1 (14.0-16.2) Gg-N yr^{-1}. While these signals are robust when averaged over several years, other factors could influence year-to-year variability in emissions, such as the El Nino-Southern Oscillation (ENSO) or the North Pacific marine heatwaves. Estimates derived from atmospheric measurements provide us with the long-term quantification not possible from sporadic ocean sampling, but future studies that also employ ocean biogeochemical models and ocean measurements would leverage a powerful combination of tools to diagnose the drivers of emissions.

We used model output from the ECCO2-Darwin model over 2009-2013 to investigate the contributions of thermally driven N_2O fluxes and those driven by ventilation using a tracer which had biogeochemical processes suppressed but with the same solubility as N_2O (Manizza et al., 2012). In the northern California EBUS, the model predicts ventilation fluxes from April to September to be around 2-4 times larger than thermal fluxes. Our findings which show that N_2O emissions correlates with both SST and upwelling, suggest that both processes could be

important. However, further model investigations run over longer time periods that span PDO phases and include important biogeochemical drivers such as pH (Breider et al., 2019) are required to determine the relative contributions of the two processes on decadal timescales. Future model work should focus on extending ocean simulations to cover both warm and cool phases of the PDO and investigate ocean pH (Breider et al., 2019), to better understand the physical and biogeochemical drivers of N_2O emissions in northern California.

2.2 Benguela (23°-35°S) and offshore South Atlantic

The location and wind patterns of NDAO makes it useful for estimating ocean trace gas fluxes from atmospheric data. We investigated the degree to which land and ocean emission contributions are separated in mole fraction measurements at NDAO. As shown in **Fig. S3**, N_2O enhancements coincide both with depleted APO as well as with low carbon monoxide (CO) mole fractions. This implies that at many of the times when the ocean upwelling source is picked up at NDAO, there is little terrestrial and anthropogenic influence.

We averaged emissions from the Benguela EBUS over all months in the period Aug 2013-Sep 2015 because wind patterns at NDAO indicate that marine emissions from coastal and offshore regions can be picked up in the atmospheric record year-round. In addition, upwelling in the northern Benguela EBUS has been shown not to exhibit significant seasonality (Chavez & Messié, 2009).

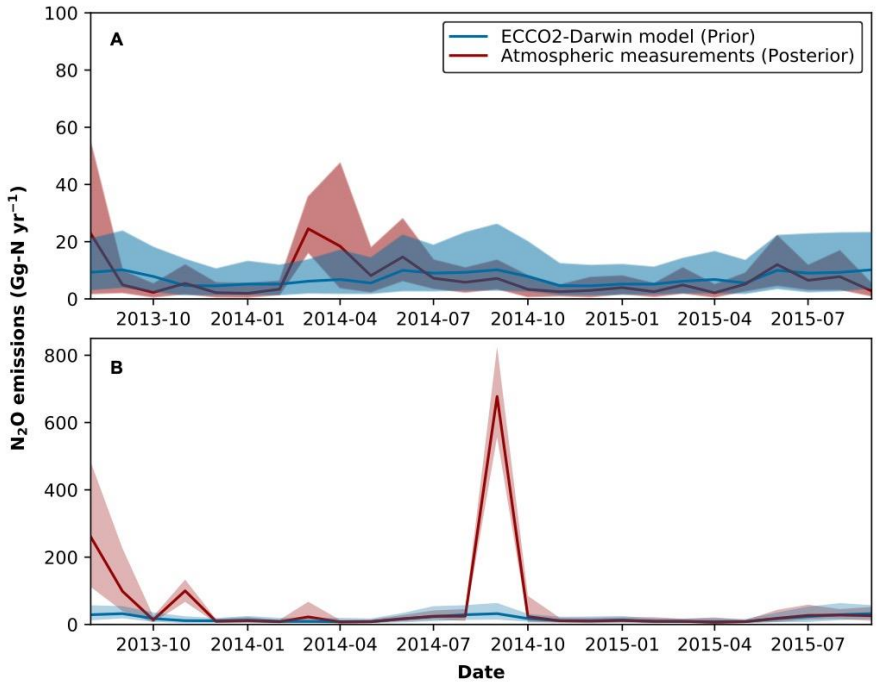

Fig. 4. Time series of offshore N_2O emissions from the South Atlantic. Emissions derived from atmospheric measurements are in red with the 95% confidence interval in red shading. *A priori* emissions and inversion uncertainty from the ocean model ECCO2-Darwin are in blue. **(a)** 150-400 km from coast and **(b)** open ocean as shown by the dotted box in **Fig. 1**.

Mean (95% confidence interval) area-integrated coastal emissions are found to be 28.4 (26.2-30.7) Gg-N yr^{-1} (**Fig. 2**). Upwelling filaments, which can transport N_2O offshore, have been found to occur 150-400 km from coast and these emissions should be considered as part of the upwelling system (Arévalo-Martínez et al., 2019). Offshore emissions 150-400 km from the coast are found to be 7.1 (5.5-9.0) Gg-N yr^{-1} (**Fig. 4**).

Our mean per-area emissions of 3.5 ng-N m^{-2} s^{-1} are around 10 times larger than the climatological fluxes derived from composite ΔpN_2O fields in (Nevison et al., 1995) (**Table S1**). However, mean emissions from August 2013 are consistent with those derived from ship-based

measurements in the same month (Morgan et al., 2019). Atmospheric measurements from NDAO were also used in (Morgan et al., 2019) to estimate upwelling emissions from the Walvis Bay and Lüderitz cells for August 2013, but estimated emissions were larger than those derived in this study and in the ship-based estimates (**Table S1**). We propose that the main reason for the lower coastal emissions estimated here using the same dataset is that the atmospheric transport model and inverse method attributes some of the NDAO N_2O mole fraction enhancements to offshore regions rather than to the coastal margin (**Fig. S4**). This finding highlights that studies that have pre-defined source regions to interpret atmospheric measurements could inaccurately quantify emissions.

Our emissions exhibit a similar spatial pattern to those derived in Arévalo-Martínez et al., (2019), with large emissions at 23°S and reduced emissions between 23°and 27°S in the Walvis Bay and Lüderitz upwelling cells (**Fig. 1**). Although measurements from other studies are not available for comparison, we find emissions south of 27°S to be of similar magnitude to those north of 23°S.

The southern boundary of the Benguela EBUS interacts with the very energetic Agulhas current, where filaments and large eddies can form offshore (Hutchings et al., 2009). Offshore emissions from this boundary region could be related to the Benguela EBUS but because of the vague boundary definition, we quantified them separately. We estimate mean area-integrated emissions from an open ocean region to the south-west of the station (**Fig. 2**) to be 56.8 (44.7-71.8) Gg-N yr^{-1} with these emissions reaching over 100 Gg-N yr^{-1} in several months and a maximum value of 677 Gg-N yr^{-1} in one month (**Fig. 4**). One possible explanation is that these emissions could be associated with mesoscale eddies, which were present in the NDAO measurement footprint during times of N_2O mole fraction enhancements (**Fig. S5**) but may not

be well-resolved in global ocean biogeochemistry models. Mesoscale eddies have been shown to have different biogeochemical properties and N_2O emissions from the surrounding ocean (Grundle et al., 2017). However, to investigate this hypothesis, future work should directly sample eddies in this region, as has been done for other EBUSs (Arévalo-Martínez et al., 2016; Grundle et al., 2017). Coupling these measurements with a longer timeseries of data from NDAO would allow for greater process-level information to be inferred.

Our results highlight the large variation in emissions from this open ocean region, which would not likely be captured by sparse measurements. The only previous ship-based measurements from this region, which occurred prior to the beginning of the measurement record used in this study, show that very large ocean N_2O mole fraction enhancements can exist (Weiss et al., 1992). These measurements show that enhancements are episodic with enhanced N_2O only found in one leg of two ship transects separated by a period of one month. Global ocean estimates using composite ΔpN_2O maps derived from these ship-based measurements could therefore substantially over- or under-estimate fluxes for such strongly variable regions.

2.3 Southern Canary (16°-23°N)

Upwelling in the southern Canary EBUS is semi-continuous (Chavez & Messié, 2009). However, our estimates are constrained by measurements only in a subset of months as discussed in **Section 2.4**. Mean (95% confidence interval) area-integrated emissions for the months during 2013-2017 that are constrained by measurements are 12.7 (10.4-15.8) Gg-N yr^{-1} (**Fig. 2**). This corresponds to mean per-area emissions of 2.7 ng-N m^{-2} s^{-1}, which is four times larger than the climatological flux shown in (Nevison et al., 1995) (**Table S1**). Our estimates show little

monthly variability and are generally consistent with ECCO2-Darwin. No measurement-based flux estimates from the time period of this study are available for direct comparison. Inclusion of APO at CVAO could help to identify whether upwelling events are occurring and are being captured at the site.

2.4 Sensitivity tests

Three sensitivity inversions were performed to test the robustness of our results: (i) Atmospheric measurements reflect the net effect of all sources and sinks of atmospheric trace gases upwind of a receptor. To demonstrate that the estimation of non-ocean sources did not significantly impact the estimation of the ocean source, we derived emissions using a subset of data that were filtered to exclude data points that were heavily influenced by anthropogenic or soil sources. The procedure for data filtering is discussed in the SI. Emissions derived from the filtered dataset (**Fig. S6**) show that results for the three EBUSs and the offshore emissions from the Benguela, are consistent with the unfiltered estimates. This finding suggests that the inversion is able to partition land and ocean sources because when some contribution of the land-based sources is removed, the inversion still estimates similar ocean emissions. (ii) We tested for the influence of the *a priori* emissions on derived emissions by scaling the total *a priori* (ocean and land) emissions by 2-10 times the original value, keeping the remainder of the methodology the same. In the northern California and Benguela regions, similar emissions were derived for all months, confirming the atmospheric constraint on the ocean source. In the southern Canary, results are consistent for a majority of months but those that are not have been excluded from the analysis (**Fig. S7**). Because the total *a priori* emissions were scaled, this resulted in a large

perturbation to emissions from the land sector, particularly for the northern California region where there are more significant land sources than in the Benguela or southern Canary regions. The consistent emissions derived for the northern California EBUS provides confidence in the ability of the inversion to separate ocean and land emissions, for if this separation were dependent on the *a priori* emissions, a large perturbation to the land emissions would affect the derived ocean emissions. (iii) We assessed the effect of the *a priori* boundary condition field on derived emissions by using two global model fields, MOZART (Emmons et al., 2010; Palmer et al., 2018) and CAMS LMDZ (Thompson, Chevallier, et al., 2014), which are discussed in the SI. We show in **Fig. S8** the prior and posterior boundary conditions at each site from the two models as well as the emissions estimated using each of these boundary conditions. These results show that emissions are consistent within uncertainties for the different boundary conditions and when offsets to the model boundary conditions are also estimated in the inversion, that a single site can constrain both boundary conditions and emissions.

We also carried out tests to investigate whether the representation of the coast in the model could have strongly impacted our results. Underlying model processes important for resolving coastal features, such as land-sea breezes, are strongly dependent on model resolution. The spatial resolution of the meteorological fields driving NAME increased from 60 km in 2003 to 12 km in 2017. The fact that emissions are being derived with similar magnitude throughout the period provides confidence in the ability of the model to partition emissions along the coastal boundary. As we aggregated our emission maps into total coastal emissions using a land-sea border that is defined at the resolution of the model grid cell, we also aggregated these emissions using different border definitions (i.e. by moving the border one or two grid cells or approximately 30-60 km inland or offshore), keeping the coastal definition the same (0-150km

337 from the border) (**Fig. S9**). The main impact on aggregated emissions using different coastal
338 boundaries is in northern California, where land sources are more significant than at the other
339 two EBUSs. Mean April-September emissions in the northern California EBUS could range
340 between 14.4-24.6 Gg-N yr^{-1}, compared to our result of 19.2 (18.5-19.9) Gg-N yr^{-1}, depending
341 on whether the border is moved one grid cell offshore or one grid cell inland. This represents an
342 extreme perturbation (i.e. a ~30 km change to the coastal boundary) but suggests that while
343 differences lie outside of the confidence interval of the main results, that a similar magnitude of
344 emissions is being derived. Differences in the other EBUSs are minimal. This experiment
345 indicates that transport model uncertainty at the coast (e.g., in representing land-sea breezes) and
346 uncertainty in coastal definition, which if significant would result in large changes when
347 aggregating emissions using different borders, do not substantially alter the conclusions of this
348 study.

349 While we show that results are not very sensitive to the land-sea partitioning, to NAME
350 transport model uncertainty at the coast or to inversion inputs such as *a priori* emissions and
351 boundary conditions, there could still be systematic uncertainties that are not accounted for.
352 These could be due to, for example, vertical mixing in NAME, the representation of the
353 planetary boundary layer or other structures in the inversion framework. Quantifying these
354 uncertainties would require models to be assessed regularly through for example, independent
355 tracer release campaigns. Model inter-comparison studies (e.g., Bergamaschi et al., 2015;
356 Thompson, Ishijima, et al., 2014; Thompson, Patra, et al., 2014) and observing system
357 simulation experiments (e.g., Wells et al., 2015) have attempted to quantify some of the
358 uncertainties in current inverse modeling capability for N_2O.
359

3 Conclusions and Discussion

The average combined coastal N_2O emissions for the three EBUSs are 50.6 (45.6-56.1) Gg-N yr^{-1} which increases to 57.7 (51.4-63.9) Gg-N yr^{-1} when including the 150-400km band of emissions from the South Atlantic. Mean emissions from each of the three EBUSs are of similar magnitude, however the largest pulses of emissions occur from the Benguela EBUS. Both the northern California and Benguela EBUSs have maximum monthly emissions that are 4-5 times greater than the mean, while there is little variability from the southern Canary. The timeseries of emissions that we derive from atmospheric measurements make it possible for the first time to quantify this variability.

Significant offshore emissions were only found in the South Atlantic near the Benguela EBUS and were not present in the eastern North Pacific or eastern tropical North Atlantic. In the South Atlantic, we identified several months with very large pulses of emissions (>600 Gg-N yr^{-1}) from an open ocean area where there could be interaction between the Benguela EBUS and the Agulhas current. These pulses are an order of magnitude larger than annual average emissions, highlighting the significant variability in these sources.

Previous studies have estimated these three EBUSs to contribute 42 Gg-N yr^{-1} for larger latitude extents than used here (Nevison et al., 2004). Our estimates do not cover more southerly extents of the California EBUS, regions north of NDAO in the Benguela or the Humboldt EBUS, and there could be important additional contributions from these areas. A study based on oceanographic measurements shows that emissions off Peru could be large (200-900 Gg-N yr^{-1}) (Arévalo-Martínez et al., 2015).

If atmospheric measurements could be implemented in the EBUSs not captured by this study as well as in open ocean regions that are influenced by the EBUSs, the method used here could quantify the magnitude and variability in these emissions over time and provide a more complete account of global ocean N_2O emissions. Measurement stations should be situated near upwelling regions and ideally, far from other sources. The primary limitation of this approach is that land-based sources need to be robustly accounted for and in some regions, these emissions may be much larger than coastal ocean emissions. Including measurements of APO and anthropogenic tracers such as CO would help to diagnose any such influences. In addition, more frequent campaigns of simultaneous ocean and atmospheric measurements would allow for regular assessment and comparison of the fluxes derived from the two methods.

Recent studies have shown that over the previous decades, ocean warming and its reduced ventilation have caused de-oxygenation and expansion of OMZs, including in the EBUSs (Oschlies et al., 2018). While responses depend on time-scales and regions, model studies predict significant changes in N_2O production and emissions in the future (Battaglia & Joos, 2018). Coupled with intensified coastal upwelling (Wang et al., 2015), increased production could lead to greater emissions to the atmosphere, re-enforcing the positive feedback between ocean biogeochemical processes and climate warming. As we have shown here, atmospheric measurements coupled with high-resolution transport modeling and an inverse method could provide us with the means to quantify any such long-term changes in the EBUSs.

401

402 **Acknowledgments and Data**

403

404 We would like to thank the station operators at Trinidad Head, Namib Desert Atmospheric
405 Observatory and Cape Verde Atmospheric Observatory for meticulous data collection over the
406 years, making this research possible. We also thank Dimitris Menemenlis and Hong Zhang for
407 providing the original code and the optimized forcing to execute numerical simulations of
408 ECCO2-Darwin to which the N_2O model code was added. Nitrous oxide and HFC-134a data
409 from THD were funded by the National Aeronautics and Space Administration (NASA) grants
410 NNX16AC96G and NNX16AC97G to the Scripps Institution of Oceanography. THD APO data
411 from 2000-2003 were funded under NASA grants NAG5-6179 and NAG5-10737. NDAO data
412 were funded by the Max Planck Society and supported by the Gobabeb Research and Training
413 Centre. CVAO data were funded by the Max Planck Society. A.G. was funded by a Natural
414 Environment Research Council (NERC) Independent Research Fellowship NE/L010992/1. M.M.
415 acknowledges the NASA Biology and Biogeochemistry grant NNX11AL73G for partial
416 financial support of this work. NAME atmospheric transport simulations for NDAO and CVAO
417 were run on the University of Bristol's Blue Crystal Phase 4 facility for high-performance
418 computing. ECCO2-Darwin simulations were carried out using the computational facilities at the
419 NASA Advanced Supercomputing Division. A.G. designed and executed the research and wrote
420 the manuscript. M.M. provided *a priori* fluxes from the ECCO2-Darwin model and advised
421 interpretation of ocean biogeochemistry. E.M. provided all data from the Namib Desert
422 Atmospheric Observatory. C.H. provided N_2O data from Trinidad Head and the AGAGE N_2O
423 calibration scale. E.K. provided all data from the Cape Verde Atmospheric Observatory. T.L.

provided APO data from Trinidad Head. A.M. provided NAME simulations for Trinidad Head. M.L. co-wrote the inversion code with A.G. J.M provided HFC-134a data from Trinidad Head. J.L. and M.H. supervised operations of NDAO and CVAO, respectively. R.W. and J.M. oversaw operations at THD and integration with AGAGE. M.R. advised on methodology. THD data are found at https://data.ess-dive.lbl.gov/view/doi:10.3334/CDIAC/ATG.DB1001 and https://agage.mit.edu/data/agage-data. CVAO data are found at https://catalogue.ceda.ac.uk/uuid/f3e7034f83e6422296d75c8a6c11da44. NDAO data are included in the Supplementary Material. Atmospheric measurements can be used by contacting Ray Weiss (rfweiss@ucsd.edu) for THD, Eric Morgan (ejmorgan@ucsd.edu) for NDAO and Elena Kozlova (E.Kozlova@exeter.ac.uk) for CVAO. THD APO measurements can be acquired through Timothy Lueker (tlueker@ucsd.edu) and ECCO2-Darwin ocean model output through Manfredi Manizza (mmanizza@ucsd.edu). Fortran 90 Code for the reversible jump MCMC inversion method and Python 3 code for running the inversion can acquired through Anita Ganesan (anita.ganesan@bristol.ac.uk).

References

Arévalo-Martínez, D. L., Kock, A., Löscher, C. R., Schmitz, R. A., & Bange, H. W. (2015). Massive nitrous oxide emissions from the tropical South Pacific Ocean. *Nature Geoscience*, *8*(7), 530–533. https://doi.org/10.1038/ngeo2469

Arévalo-Martínez, D. L., Kock, A., Löscher, C. R., Schmitz, R. A., Stramma, L., & Bange, H. W. (2016). Influence of mesoscale eddies on the distribution of nitrous oxide in the eastern tropical South Pacific. *Biogeosciences*, *13*(4), 1105–1118. https://doi.org/10.5194/bg-13-1105-2016

Arévalo-Martínez, D. L., Steinhoff, T., Brandt, P., Körtzinger, A., Lamont, T., Rehder, G., & Bange, H. W. (2019). N_2O Emissions From the Northern Benguela Upwelling System. *Geophysical Research Letters*, *46*(6), 3317–3326. https://doi.org/10.1029/2018GL081648

Battaglia, G., & Joos, F. (2018). Marine N_2O Emissions From Nitrification and Denitrification Constrained by Modern Observations and Projected in Multimillennial Global Warming Simulations. *Global Biogeochemical Cycles*, *32*(1), 92–121. https://doi.org/10.1002/2017GB005671

Bergamaschi, P., Corazza, M., Karstens, U., Athanassiadou, M., Thompson, R. L., Pison, I., et al. (2015). Top-down estimates of European CH₄ and N₂O emissions based on four different inverse models. *Atmospheric Chemistry and Physics*, *15*(2), 715–736. https://doi.org/10.5194/acp-15-715-2015

Breider, F., Yoshikawa, C., Makabe, A., Toyoda, S., Wakita, M., Matsui, Y., et al. (2019). Response of N_2O production rate to ocean acidification in the western North Pacific. *Nature Climate Change*, *9*(12), 954–958. https://doi.org/10.1038/s41558-019-0605-7

Buitenhuis, E. T., Suntharalingam, P., & Le Quéré, C. (2018). Constraints on global oceanic emissions of N₂O from observations and models. *Biogeosciences*, *15*(7), 2161–2175. https://doi.org/10.5194/bg-15-2161-2018

Capelle, D. W., & Tortell, P. D. (2016). Factors controlling methane and nitrous-oxide variability in the southern British Columbia coastal upwelling system. *Marine Chemistry*, *179*, 56–67. https://doi.org/10.1016/j.marchem.2016.01.011

Capone, D. G., & Hutchins, D. A. (2013). Microbial biogeochemistry of coastal upwelling regimes in a changing ocean. *Nature Geoscience*, *6*(9), 711–717. https://doi.org/10.1038/ngeo1916

Chavez, F. P., & Messié, M. (2009). A comparison of Eastern Boundary Upwelling Ecosystems. *Progress in Oceanography*, *83*(1–4), 80–96. https://doi.org/10.1016/j.pocean.2009.07.032

Ciais, P., Sabine, C., Bala, G., Bopp, L., Brovkin, V., Canadell, J. G., et al. (2013). Carbon and Other Biogeochemical Cycles. In: Climate Change 2013: The Physical Science Basis. Contribution of Working Group I to the Fifth Assessment Report of the Intergovernmental Panel on Climate Change, [Stocker, T.F., D. Qin, G.-K. Plattner, M. Tignor, S.K. Allen, J. Boschung, A. Nauels, Y. Xia, V. Bex and P.M. Midgley (eds.)], Cambridge University Press, Cambridge, United Kingdom and New York, NY, USA.

Emmons, L. K., Walters, S., Hess, P. G., Guenther, A., Kinnison, D., Laepple, T., et al. (2010). Description and evaluation of the Model for Ozone and Related chemical Tracers, version 4 (MOZART-4). *Geosci. Model Dev.*, 25. https://doi.org/10.5194/gmd-3-43-2010

Fenwick, L., & Tortell, P. D. (2018). Methane and nitrous oxide distributions in coastal and open ocean waters of the Northeast Subarctic Pacific during 2015–2016. *Marine Chemistry*, *200*, 45–56. https://doi.org/10.1016/j.marchem.2018.01.008

Frame, C. H., Deal, E., Nevison, C. D., & Casciotti, K. L. (2014). N_2O production in the eastern South Atlantic: Analysis of N_2O stable isotopic and concentration data. *Global Biogeochemical Cycles*, *28*(11), 1262–1278. https://doi.org/10.1002/2013GB004790

Ganesan, A. L., Rigby, M., Zammit-Mangion, A., Manning, A. J., Prinn, R. G., Fraser, P. J., et al. (2014). Characterization of uncertainties in atmospheric trace gas inversions using hierarchical Bayesian methods. *Atmospheric Chemistry and Physics*, *14*(8), 3855–3864. https://doi.org/10.5194/acp-14-3855-2014

Grundle, D. S., Löscher, C. R., Krahmann, G., Altabet, M. A., Bange, H. W., Karstensen, J., et al. (2017). Low oxygen eddies in the eastern tropical North Atlantic: Implications for N_2O cycling. *Scientific Reports*, *7*(1), 1–10. https://doi.org/10.1038/s41598-017-04745-y

Hutchings, L., van der Lingen, C. D., Shannon, L. J., Crawford, R. J. M., Verheye, H. M. S., Bartholomae, C. H., et al. (2009). The Benguela Current: An ecosystem of four components. *Progress in Oceanography*, *83*(1), 15–32. https://doi.org/10.1016/j.pocean.2009.07.046

Huyer, A. (1983). Coastal upwelling in the California current system. *Progress in Oceanography*, *12*(3), 259–284. https://doi.org/10.1016/0079-6611(83)90010-1

Janssens-Maenhout, G., Crippa, M., Guizzardi, D., Muntean, M., Schaaf, E., Dentener, F., et al. (2019). EDGAR v4.3.2 Global Atlas of the three major greenhouse gas emissions for the period 1970–2012. *Earth System Science Data*, *11*(3), 959–1002. https://doi.org/10.5194/essd-11-959-2019

Jones, A., Thomson, D., Hort, M., & Devenish, B. (2006). The U.K. Met Office's Next-Generation Atmospheric Dispersion Model, NAME III. In C. Borrego & A.-L. Norman (Eds.), *Air Pollution Modeling and Its Application XVII* (pp. 580–589). Boston, MA: Springer US. https://doi.org/10.1007/978-0-387-68854-1_62

Kock, A., Gebhardt, S., & Bange, H. W. (2008). Methane emissions from the upwelling area off Mauritania (NW Africa). *Biogeosciences*, *5*(4), 1119–1125. https://doi.org/10.5194/bg-5-1119-2008

Lueker, T. J. (2004). Coastal upwelling fluxes of O_2, N_2O, and CO_2 assessed from continuous atmospheric observations at Trinidad, California. *Biogeosciences*, *1*(1), 101–111. https://doi.org/10.5194/bg-1-101-2004

Lueker, T. J., Walker, S. J., Vollmer, M. K., Keeling, R. F., Nevison, C. D., Weiss, R. F., & Garcia, H. E. (2003). Coastal upwelling air-sea fluxes revealed in atmospheric observations of O_2/N_2, CO_2 and N_2O. *Geophysical Research Letters*, *30*(6). https://doi.org/10.1029/2002GL016615

Lunt, M. F., Rigby, M., Ganesan, A. L., & Manning, A. J. (2016). Estimation of trace gas fluxes with objectively determined basis functions using reversible-jump Markov chain Monte Carlo. *Geoscientific Model Development*, *9*(9), 3213–3229. https://doi.org/10.5194/gmd-9-3213-2016

Manizza, M., Keeling, R. F., & Nevison, C. D. (2012). On the processes controlling the seasonal cycles of the air–sea fluxes of O_2 and N_2O: A modelling study. *Tellus B: Chemical and Physical Meteorology*, *64*(1), 18429. https://doi.org/10.3402/tellusb.v64i0.18429

Manizza, M., Menemenlis, D., Zhang, H., & Miller, C. E. (2019). Modeling the Recent Changes in the Arctic Ocean CO_2 Sink (2006–2013). *Global Biogeochemical Cycles*, *33*(3), 420–438. https://doi.org/10.1029/2018GB006070

Mantua, N. J., Hare, S. R., Zhang, Y., Wallace, J. M., & Francis, R. C. (1997). A Pacific Interdecadal Climate Oscillation with Impacts on Salmon Production. *Bulletin of the American Meteorological Society*, *78*(6), 1069–1080. https://doi.org/10.1175/1520-0477(1997)078<1069:APICOW>2.0.CO;2

Morgan, E. J., Lavrič, J. V., Seifert, T., Chicoine, T., Day, A., Gomez, J., et al. (2015). Continuous measurements of greenhouse gases and atmospheric oxygen at the Namib Desert Atmospheric Observatory. *Atmospheric Measurement Techniques*, *8*(6), 2233–2250. https://doi.org/10.5194/amt-8-2233-2015

Morgan, E. J., Lavric, J. V., Arévalo-Martínez, D. L., Bange, H. W., Steinhoff, T., Seifert, T., & Heimann, M. (2019). Air–sea fluxes of greenhouse gases and oxygen in the northern Benguela Current region during upwelling events. *Biogeosciences*, *16*(20), 4065–4084. https://doi.org/10.5194/bg-16-4065-2019

Myhre, G., Shindell, D., Bréon, F.-M., Collins, W., Fuglestvedt, J., Huang, J., et al. (2013). Anthropogenic and Natural Radiative Forcing. In: Climate Change 2013: The Physical Science Basis. Contribution of Working Group I to the Fifth Assessment Report of the Intergovernmental Panel on Climate Change, [Stocker, T.F., D. Qin, G.-K. Plattner, M. Tignor, S.K. Allen, J. Boschung, A. Nauels, Y. Xia, V. Bex and P.M. Midgley (eds.)], Cambridge University Press, Cambridge, United Kingdom and New York, NY, USA.

Naqvi, S. W. A., Bange, H. W., Farías, L., Monteiro, P. M. S., Scranton, M. I., & Zhang, J. (2010). Marine hypoxia/anoxia as a source of CH_4 and N_2O. *Biogeosciences*, *7*(7), 2159–2190. https://doi.org/10.5194/bg-7-2159-2010

Nevison, C. D., Weiss, R. F., & Erickson, D. J. (1995). Global oceanic emissions of nitrous oxide. *Journal of Geophysical Research*, *100*(C8), 15809. https://doi.org/10.1029/95JC00684

Nevison, C. D., Butler, J. H., & Elkins, J. W. (2003). Global distribution of N_2O and the ΔN_2O-AOU yield in the subsurface ocean. *Global Biogeochemical Cycles*, *17*(4), n/a-n/a. https://doi.org/10.1029/2003GB002068

Nevison, C. D., Lueker, T. J., & Weiss, R. F. (2004). Quantifying the nitrous oxide source from coastal upwelling. *Global Biogeochemical Cycles*, *18*(1). https://doi.org/10.1029/2003GB002110

NOAA Southwest Fisheries Science Center. (n.d.). https://oceanview.pfeg.noaa.gov/products/upwelling/, accessed 9 December 2019.

Oschlies, A., Brandt, P., Stramma, L., & Schmidtko, S. (2018). Drivers and mechanisms of ocean deoxygenation. *Nature Geoscience*, *11*(7), 467–473. https://doi.org/10.1038/s41561-018-0152-2

Palmer, P. I., O'Doherty, S., Allen, G., Bower, K., Bösch, H., Chipperfield, M. P., et al. (2018). A measurement-based verification framework for UK greenhouse gas emissions: an overview of the Greenhouse gAs Uk and Global Emissions (GAUGE) project. *Atmospheric Chemistry and Physics*, *18*(16), 11753–11777. https://doi.org/10.5194/acp-18-11753-2018

Prinn, R. G., Weiss, R. F., Arduini, J., Arnold, T., DeWitt, H. L., Fraser, P. J., et al. (2018). History of chemically and radiatively important atmospheric gases from the Advanced Global Atmospheric Gases Experiment (AGAGE). *Earth System Science Data*, *10*(2), 985–1018. https://doi.org/10.5194/essd-10-985-2018

Ravishankara, A. R., Daniel, J. S., & Portmann, R. W. (2009). Nitrous Oxide (N_2O): The Dominant Ozone-Depleting Substance Emitted in the 21st Century. *Science*, *326*(5949), 123–125. https://doi.org/10.1126/science.1176985

Saikawa, E., Schlosser, C. A., & Prinn, R. G. (2013). Global modeling of soil nitrous oxide emissions from natural processes. *Global Biogeochemical Cycles*, *27*(3), 972–989. https://doi.org/10.1002/gbc.20087

Thompson, R. L., Chevallier, F., Crotwell, A. M., Dutton, G., Langenfelds, R. L., Prinn, R. G., et al. (2014). Nitrous oxide emissions 1999 to 2009 from a global atmospheric inversion. *Atmospheric Chemistry and Physics*, *14*(4), 1801–1817. https://doi.org/10.5194/acp-14-1801-2014

Thompson, R. L., Patra, P. K., Ishijima, K., Saikawa, E., Corazza, M., Karstens, U., et al. (2014). TransCom N_2O model inter-comparison – Part 1: Assessing the influence of transport and surface fluxes on tropospheric N_2O variability. *Atmospheric Chemistry and Physics*, *14*(8), 4349–4368. https://doi.org/10.5194/acp-14-4349-2014

Thompson, R. L., Ishijima, K., Saikawa, E., Corazza, M., Karstens, U., Patra, P. K., et al. (2014). TransCom N₂O model inter-comparison – Part 2: Atmospheric inversion estimates of N₂O emissions. *Atmospheric Chemistry and Physics*, *14*(12), 6177–6194. https://doi.org/10.5194/acp-14-6177-2014

Wang, D., Gouhier, T. C., Menge, B. A., & Ganguly, A. R. (2015). Intensification and spatial homogenization of coastal upwelling under climate change. *Nature*, *518*(7539), 390–394. https://doi.org/10.1038/nature14235

Wanninkhof, R. (1992). Relationship between wind speed and gas exchange over the ocean. *Journal of Geophysical Research: Oceans*, *97*(C5), 7373–7382. https://doi.org/10.1029/92JC00188

Weiss, R. F., Van Woy, F. A., Salameh, P. K. (Scripps I. of O., & Sepanski, R. J. (Tennessee U. (1992). *Surface water and atmospheric carbon dioxide and nitrous oxide observations by shipboard automated gas chromatography: Results from expeditions between 1977 and 1990* (No. ORNL/CDIAC-59; SIO--92-11; NDP--044). Oak Ridge National Lab., TN (United States). Carbon Dioxide Information Analysis Center. https://doi.org/10.2172/6726159

Wells, K. C., Millet, D. B., Bousserez, N., Henze, D. K., Chaliyakunnel, S., Griffis, T. J., et al. (2015). Simulation of atmospheric N_2O with GEOS-Chem and its adjoint: evaluation of observational constraints. *Geoscientific Model Development*, *8*(10), 3179–3198. https://doi.org/10.5194/gmd-8-3179-2015

Wittke, F., Kock, A., & Bange, H. W. (2010). Nitrous oxide emissions from the upwelling area off Mauritania (NW Africa). *Geophysical Research Letters*, *37*(12), L12601. https://doi.org/10.1029/2010GL042442